

PART III: HYDRODYNAMICS ASPECTS OF THE ELECTROKINETIC REMEDIATION PROCESS IN THE TREATMENT ZONE: ELECTRO-MECHANISMS AND JOULE HEATING

Chapter V. Rectangular Geometry: Effect of Asymmetry (W_{∞})

5.1 Introduction and Motivation

This chapter focuses on the analysis of the combined influence of Joule heating generation with electroosmosis and under the action of a pressure gradient. As far as it is known, this is the first systematic analysis based on the application of the fundamental equations of electrokinetic transport to determine *a priori* design criteria and apply these to show the effect of key parameters in controlling flow behavior. The goal here is rather modest and it seeks the understanding of the different flow regimes that may be possible in a rectangular channel. Furthermore, operational parameters are identified and their role in the determination of the flows studied. In order to accomplish these objectives, several simplifying assumptions are made to capture the dominating aspects and in order to have a manageable description of the system from an analytical point of view. The most important objective of this study is to obtain a qualitative and semi-quantitative description of the different flow regimes inside a rectangular channel. The role of the wall temperatures of the capillary on the velocity field is also studied. This information is not only useful to identify further aspects for the investigation but also to delineate a systematic approach for a more rigorous description. More specifically, the idea behind the study is to promote a deeper understanding of the behavior of the system and to have a better idea about the experimental

effort needed for validation of the different trends. The chapter has been divided in several sections that include the description of the temperature profile and the hydrodynamic velocity profile. A discussion of the different flow regimes and their implication to the behavior of the system follows. Finally, some general suggestions for further research are included.

5.2 Model Formulation

The system under analysis consists of a channel of length L , width $2B$ and an inclination of an angle α with respect to the horizontal line as described in figure 5.1 below.

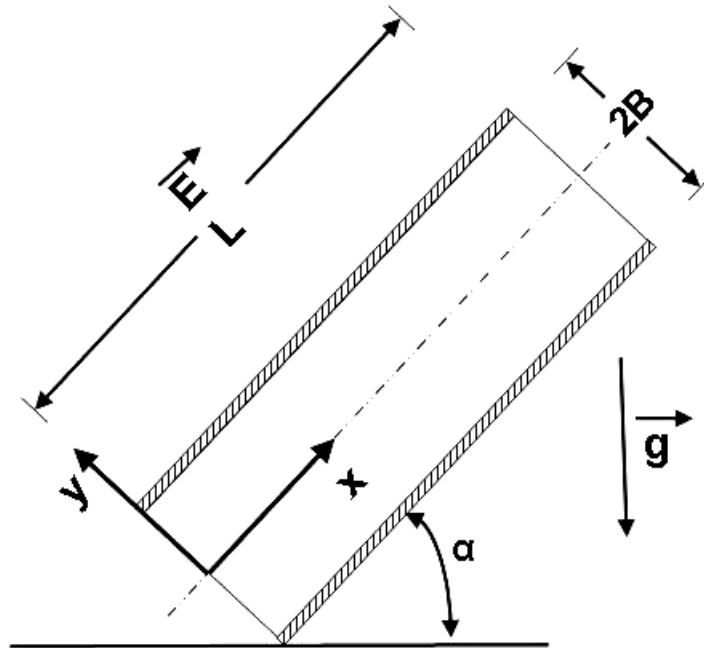


Figure 5.1 Geometrical sketch of the rectangular capillary channel and coordinate system used in the analysis.

The channel is exposed to an electrical field E . The walls of the channel have a net but constant and uniform charge. The walls may present either equal or different temperatures as

defined by their interaction with the temperature of the surroundings. The fact that they may be equal or not, leads to a presence of a symmetrical condition in the temperature profile that will be closely studied here. The axes (x and y) have been placed coincidentally with the lower end of the capillary channel, x , and the origin of the y -axis at the middle of channel. This choice of the coordinate axis simplifies the algebra considerably as will be shown in the later sections.

The mathematical description of the system calls for the analysis of at least three main aspects, i.e., heat transfer, electrostatics, and hydrodynamics. Each aspect yields a profile of a relevant variable for the study of the system behavior. For example, the electrostatic potential is determined by the conservation of charge in the system; the temperature profile is originated in the heat transfer of the system with its surroundings; and, finally, the hydrodynamics leads to the velocity profile that controls the different flows. In the sections below, the description of these two last different aspects is included as the electrostatic model was widely discussed in Part II.

5.2.1 Heat Transfer Model

The channel (see figure 5.1) is assumed to interchange heat with its surroundings within a range of efficiencies, i.e., the Nusselt number may take values within a wide spectrum of possibilities. This situation may also lead to the situation in which the temperature of the walls of the channel at the positions $y = -B$ and $y = +B$ reach the values of temperature of their environments; these values are considered to be constant. In addition, the ratio B/L is assumed small enough to neglect any end effects on the temperature profile inside the channel. Furthermore, the conduction-dominated regime (Batchelor, 1954) is assumed valid for the present analysis. An applied electrical field E in the axial direction (i.e., the x -axis) of the channel is present and due to the fact that the fluid inside the channel shows a non-zero resistance to the electrical current, heat generation takes place. This is known as the Joule heating generation, Q , and, for this study it is assumed constant with time and uniform across the channel. Under the assumptions just described, the energy equation (Bird et al., 1960) reduces to:

$$-\frac{\partial}{\partial \xi} \left(\frac{\partial \theta}{\partial \xi} \right) \equiv \phi^2 \quad (5.1)$$

The following definitions have been used for the non-dimensional variables:

$$\xi \equiv \frac{y}{B}; \quad \theta \equiv \frac{(T - T_\infty)}{T_\infty} \quad (5.2)$$

and the Joule heating number has been identified as:

$$\phi^2 \equiv \frac{Q \cdot B^2}{KT_\infty} \quad (5.3)$$

where, Q is the Joule heating generation, K the thermal conductivity of the fluid of the channel, and T_∞ the temperature of the channel environment at the right side wall, this is at $y=+B$.

The conservation of energy equation 5.1 needs boundary conditions at both walls of the channel; although different types of boundary conditions are possible (Incropera, 1996; Boland et al., 2000) in this analysis we are interested in a simple case. Therefore, the flux or Robin boundary conditions (Incropera, 1996) are selected at the walls of the capillary channel and they are given by the following equations:

$$\left. \frac{\partial \theta}{\partial \xi} \right|_{\xi=-1} = Nu \cdot \left(\theta \right)_{\xi=-1} + W_\infty \quad @ \quad \xi = -1 \quad (5.4a)$$

$$-\left. \frac{\partial \theta}{\partial \xi} \right|_{\xi=+1} = Nu \cdot \left(\theta \right)_{\xi=+1} \quad @ \quad \xi = +1 \quad (5.4b)$$

In the previous expression, Equation 5.4a, the term W_∞ appears. This term has been named the “*Asymmetric or Skew Factor*” since it accounts for uneven values of the surrounding temperatures. The asymmetric factor is defined as

$$W_\infty = 1 - \frac{T_\infty^*}{T_\infty} \quad (5.5)$$

where T_∞^* and T_∞ are the temperature of the channel environment at the left ($y = -B$) and right side ($y = +B$) walls respectively. The role of this factor on the behavior of the temperature and hydrodynamic velocity profiles will be examined.

The solution to the differential model for the heat transfer described by equation 5.1 and boundary conditions equation 5.4 a&b is readily computed as:

$$\theta(\xi) = -\phi^2 \left(\frac{\xi^2}{2} \right) + \frac{W_\infty}{\left[1 + \frac{1}{N_u} \right]} \left(\frac{\xi}{2} \right) + \frac{1}{N_u} \phi^2 + \frac{\phi^2}{2} - \frac{W_\infty}{2} \quad (5.6)$$

Equation 5.6 is written in terms of the skew or asymmetric factor, W_∞ , identified above. As mentioned previously, this factor accounts for uneven values of the surrounding temperatures and it is related to the linear term of the temperature profile and, therefore, it handles the asymmetric part of the function. A value of $W_\infty=0$ in equation 5.6 renders this equation to a completely symmetrical function. This fact will have implications to the hydrodynamic velocity profile, as it will be seen in a later section. In addition, equation 5.6 is an analytical function of the position of channel, across the two walls, and it is very useful in the computation of the hydrodynamic velocity profile to be described in a section below. Furthermore, equation 5.6 yields some interesting limiting cases. For example, the situation of a high convective cooling system leads to:

$$\theta(\xi) = -\phi^2 \left(\frac{\xi^2}{2} \right) + W_\infty \left(\frac{\xi}{2} \right) + \frac{\phi^2}{2} - \frac{W_\infty}{2} \quad (5.7a)$$

and for any Nussel number value, the minimum temperature is located at the wall exposed to the environment with the lowest temperature, $\xi=1$. This is:

$$\theta_{\text{MIN}} = \frac{W_{\infty}}{\left[1 + \frac{1}{N_u}\right]} \left(\frac{1}{2}\right) + \frac{1}{N_u} \phi^2 - \frac{W_{\infty}}{2} \quad (5.7b)$$

This situation produces the lowest temperature in the system for any value of the Joule heating parameter, ϕ^2 , and a given W_{∞} . Also, the temperature difference between any value and the lowest value is readily given by:

$$\Delta\theta(\xi) = -\phi^2 \left(\frac{\xi}{2}\right)^2 + \frac{W_{\infty}}{\left[1 + \frac{1}{N_u}\right]} \cdot \left(\frac{\xi}{2} - \frac{1}{2}\right) + \frac{1}{2} \phi^2 \quad (5.7c)$$

This equation becomes useful to predict temperature differences between the central location of the capillary channel and the surface of such domain. This is given by the following simple relation:

$$\Delta\theta(\xi) = \frac{W_{\infty}}{\left[1 + \frac{1}{N_u}\right]} \cdot \left(-\frac{1}{2}\right) + \frac{1}{2} \phi^2 \quad (5.7d)$$

For the symmetrical case, $W_{\infty}=0$, the temperature difference given by equation 5.7d depends solely on the Joule heating parameter, ϕ^2 . Clearly, for the case of no Joule heating generation, no temperature difference is present in the system.

5.2.2 Hydrodynamic Model

The carrier fluid involved in the flow in the channel described in figure 5.1 is a Newtonian fluid under incompressible conditions for the mass conservation aspects. This fluid is assumed to have constant properties everywhere except for the density in the buoyancy force term. This is, in fact, the assumption suggested by Boussinesq (Gebhardt et al., 1988). All the assumptions described in the previous section, above, are assumed valid for the hydrodynamic flow problem as well. In particular, the “no end effects” and the conduction-dominated regime (i.e., small magnitude of velocity field) are invoked here. Moreover, a pressure gradient is assumed to be present but its magnitude must be relatively small to comply with the assumption of a small velocity field. Under these assumptions, the axial or x-component of the Navier-Stokes equation (Bird et al., 1960) is given by

$$\mu \cdot \frac{\partial^2 V_x}{\partial y^2} = \frac{\partial p}{\partial x} - \rho(T) \cdot g_x - \rho_e(\psi) \cdot E_x \quad (5.8)$$

where the applied electrical field in the axial direction, E_x , is assumed constant and the function $\rho(T)$ is computed by a first order Taylor approximation around a mean temperature T_m of the system (Bird et al., 1960)

$$\rho(T) = \rho(T_m) - \beta_m \rho_m (T - T_m) \quad (5.9)$$

The parameter T_m is determined by the total mass conservation condition that may be stated as

$$\int_{-B}^{+B} \rho(T_m) \cdot V_x(y, T_m) \cdot dy = 0 \quad (5.10a)$$

or, as a dimensionless equation

$$\int_{-1}^{+1} \rho_m \cdot V_x^+(\xi, \theta_m) \cdot d\xi = 0 \quad (5.10b)$$

The condition given by Equation 5.10 requires the computation of the hydrodynamic velocity profile previously to its solution. Finally, the function ρ_e , electrostatic density, is defined by the following expression

$$\rho_e = -\frac{\varepsilon \cdot k^2}{4 \cdot \pi} \cdot \psi(\xi) \quad (5.11)$$

where ε is the media permittivity and k is inverse of the Debye length.

Equation 5.11 features the electrostatic potential, $\psi(\xi)$, that is obtained by solving the Debye-Hückel equation and modified by $f_{\Lambda O}$, the Correction Function, as it was described in the Part II, chapter III of this thesis.

In order to have a convenient way of analyzing the different aspects related to the velocity profile $V_x(y)$, the following dimensionless variables and numbers are proposed.

$$V_E = \frac{E_x \cdot \varepsilon \cdot \psi_w}{4 \cdot \pi \cdot \mu} \quad (5.12a)$$

$$V_x^+ = \frac{V_x}{V_E} \quad (5.12b)$$

$$G_r = \frac{\beta_m \cdot \rho_m^2 \cdot B^3 \cdot T_\infty \cdot g}{\mu^2} \quad (5.12c)$$

$$G_r^* = \beta_m \cdot T_\infty \cdot G_r \quad (5.12d)$$

$$R_e = \frac{V_E \cdot B \cdot \rho_m}{\mu} \quad (5.12e)$$

$$P_m = \frac{\partial h_p}{\partial x} \cdot \frac{G_r^*}{R_e} + \sin(\alpha) \cdot \frac{G_r^*}{R_e} \quad (5.12f)$$

The Grashoff numbers, Gr and Gr^* , represent the buoyancy to viscous forces due to changes in temperature and density respectively, while in Equation 5.12e, the Reynolds number, Re , represents the inertia to viscous forces. A convenient combination of Grashoff and Reynolds numbers has been mathematically applied to dimensionally reduce the total hydraulic head gradient, which yields the dimensionless number P_m shown by equation 5.12f. By using these numbers and variables in the Navier-Stokes component, equation 5.8, the following dimensionless differential equation is obtained

$$\frac{\partial}{\partial \xi} \left(\frac{\partial v_x^+}{\partial \xi} \right) = P_m - \frac{Gr}{R_e} \cdot \sin(\alpha) \cdot (\theta - \theta_m) + \lambda^2 \frac{\psi(\xi)}{\psi_w} \quad (5.13)$$

This equation shows several terms that account for the different forces present in the system. The left side of the equation is the viscous term, the first term on the right side represents the pressure driven force, the second is related to the buoyancy effects, and the last one is associated with the electroosmosis term.

In order to complete the problem for the electro-hydrodynamic velocity profile, the non slip-boundary conditions will be assumed at both walls of the channel:

$$V_x^+(\xi) \Big|_{\xi=-1} = 0 \quad @ \quad \xi = -1 \quad (5.14a)$$

$$V_x^+(\xi) \Big|_{\xi=+1} = 0 \quad @ \quad \xi = +1 \quad (5.14b)$$

Equation 5.13 can be trivially solved by simple substitution of the temperature and electrostatic potential profile equations followed by mathematical integration and constants' evaluation using the boundary conditions of equations 5.14 a&b. The solution, after applications of the non-slip boundary conditions have been used, yields

$$V^+_x(\xi) = A_0 \cdot (\xi^2 - 1) - A_1(\xi^3 - \xi) + A_2 \cdot (\xi^4 - 1) - 2 \cdot \left\{ \frac{\cosh(\lambda\xi)}{\cosh(\lambda)} - 1 \right\} \quad (5.15)$$

where, the following parameters have been identified in the function above:

$$A_0 = P_m - \frac{G_r}{R_e} \cdot \sin(\alpha) \cdot \left[\frac{1}{Nu} \cdot \phi^2 + \frac{1}{2} \cdot \phi^2 - \frac{1}{2} \cdot W_\infty - \theta_m \right] \quad (5.16a)$$

$$A_1 = \frac{G_r}{R_e} \cdot \sin(\alpha) \cdot \frac{W_\infty}{12 \cdot \left(\frac{1}{Nu} + 1 \right)} \quad (5.16b)$$

$$A_2 = \frac{G_r}{R_e} \cdot \sin(\alpha) \cdot \frac{1}{24} \cdot \phi^2 \quad (5.16c)$$

An interesting observation is that the parameter A_1 becomes a direct function of the skew factor, W_∞ and for the value of $W_\infty=0$ the asymmetrical term in the velocity profile becomes zero. This fact renders the velocity profile to a completely symmetrical function.

5.2.3 The Mass Conservation Condition

The mean temperature, T_m , or its equivalent dimensionless form, θ_m , was used to expand in Taylor's series the term density, equation 5.9, since it is affected by temperature changes inducing buoyancy. As was stated, the mass conservation condition, equation 5.10, required the knowledge of the hydrodynamic velocity to compute the system mean temperature. Now that such expression has been obtained, equation 5.15, the mass conservation equation can be solved for the dimensionless mean temperature, θ_m . The expression in this case corresponds to:

$$\theta_m = \frac{3 \cdot \{ \tanh(\lambda) - 1 \} - P_m}{\frac{G_r}{R_e} \cdot \sin(\alpha)} + \frac{1}{Nu} \cdot \phi^2 + \frac{9}{20} \cdot \phi^2 - \frac{W_\infty}{2} \quad (5.17)$$

This function is related to all the important parameters in the system. Thus, equation (5.17) is a function of the dimensionless hydraulic pressure gradient, P_m , the Nusselt number, N_u , the modified Debye length, λ , the Joule heating generation number, ϕ^2 , the asymmetric factor, W_∞ , the inclination angle, α , the Grashoff number, Gr , and Reynolds number, Re . In addition, θ_m is a linear function of the parameter P_m , the Reynolds number, Re , and Joule heating generation, ϕ^2 , as well as of the skew factor W_∞ . In contrast, θ_m is an hyperbolic function of both the N_u and the Grashoff number, Gr , as well as of the inclination angle, α . The dimensionless Debye length, λ , is present through a non-linear trigonometric relationship.

5.3 Design Criteria

In order to compute meaningful numerical values for the temperature and velocity profiles, a number of new criteria must be developed. This is first accomplished by restricting the range of feasible Joule heating generation number, ϕ^2 , to those values that do not imply a change in the fluid phase. Under ambient conditions change of phase will occur at temperature values of approximately $\theta \geq 0.24$ yielding a range of the Joule heating generation number of $0 \leq \phi^2 \leq 0.4$. This criterion is implicit in all the calculations herein presented. Another physical constraint taken into consideration is that the mean temperature can not exceed the maximum temperature in the system. By using this physical constraint, a range of feasible values for the dimensionless hydraulic head gradient has been derived. In particular, equations (5.18a) and (5.18b) are used to identify the location of maximum temperature and its value respectively.

$$\xi_{MAX} = \frac{1}{2 \cdot \phi^2} \cdot \frac{W_\infty}{\left(1 + \frac{1}{N_u}\right)} \quad (5.18a)$$

$$\theta_{MAX} = \frac{1}{8} \cdot \frac{1}{\phi^2} \cdot \left(\frac{W_\infty}{1 + \frac{1}{N_u}}\right)^2 + \frac{1}{N_u} \cdot \phi^2 + \frac{1}{2} \cdot \phi^2 - \frac{W_\infty}{2} \quad (5.18b)$$

On the other hand, equations (5.19a) and (5.19b), given below, are used to identify the location of minimum temperature and its value respectively.

$$\xi_{\text{MIN}} = +1 \quad (5.19a)$$

$$\theta_{\text{MIN}} = \frac{W_{\infty}}{2 \cdot \left(1 + \frac{1}{\text{Nu}}\right)} + \frac{1}{\text{Nu}} \cdot \phi^2 - \frac{W_{\infty}}{2} \quad (5.19b)$$

By using the expressions for maximum and minimum temperature in the system, equations (5.18b) and (5.19b), in combination with the expression for the mean temperature, equation (5.17), the following dimensionless hydraulic head gradient criteria are established.

$$\text{Pm}_{\text{MIN}} = 3 \cdot \{\tanh(\lambda) - 1\} - \frac{G_r}{R_e} \cdot \sin(\alpha) \cdot \left\{ \frac{\phi^2}{20} + \frac{1}{8 \cdot \phi^2} \cdot \left(\frac{W_{\infty}}{1 + \frac{1}{\text{Nu}}} \right)^2 \right\} \quad (5.20)$$

$$\text{Pm}_{\text{MAX}} = 3 \cdot \{\tanh(\lambda) - 1\} + \frac{G_r}{R_e} \cdot \sin(\alpha) \cdot \left\{ \frac{9}{20} \phi^2 - \frac{W_{\infty}}{2 \cdot \left(1 + \frac{1}{\text{Nu}}\right)} \right\} \quad (5.21)$$

The use of these design equations is very practical to identify parameter values for the numerical illustration that is presented in the next section. Once again, the criteria represented by equations (5.20) and (5.21) are implicit in all the calculations herein presented.

5.4 Illustrative Results and Discussion

Figure 5.2 (a&b) shows the temperature profile for two limiting cases of the asymmetric factor, W_{∞} , with the Joule heating number, ϕ^2 , as a parameter ranging between the values of 0.02 and 0.40. By comparing figures 5.2a and 5.2b it is clearly observed the important role of the asymmetric factor; for example, in the case of $W_{\infty} \neq 0$ there is a “lifting” effect on all the temperature values starting at position $\xi=-1$ and gradually vanishing toward the position $\xi=+1$.

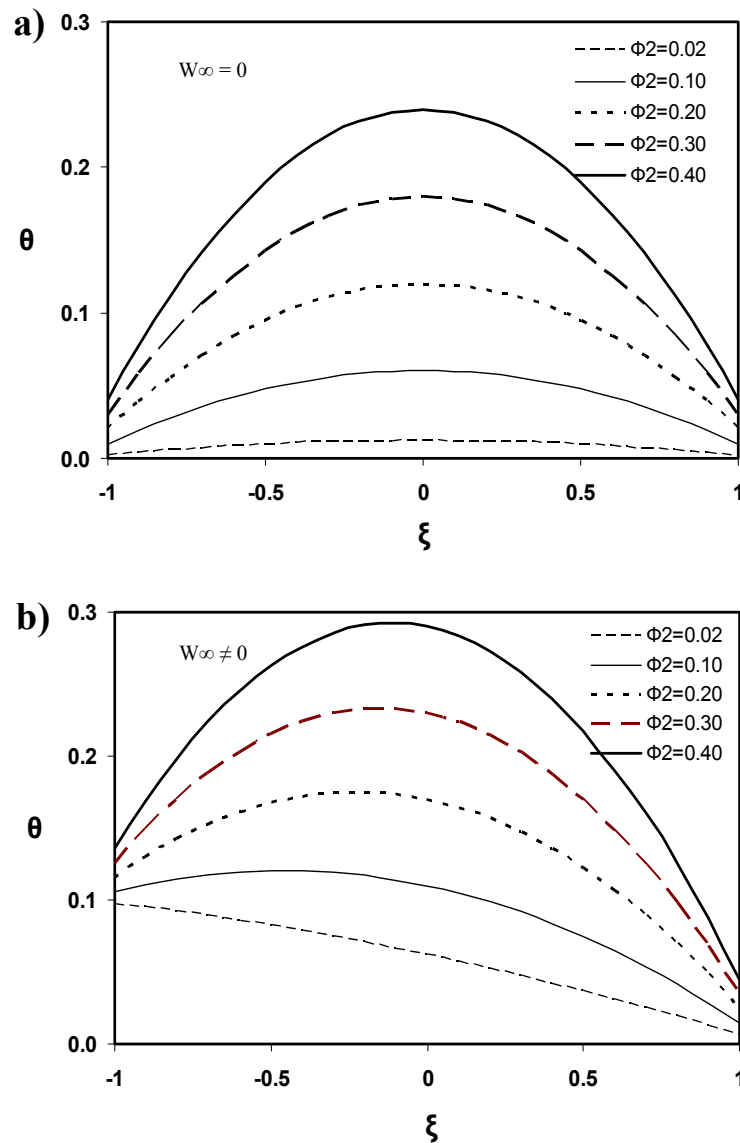


Figure 5.2 Dimensionless temperature profiles (inside the capillary channel) for the *symmetrical case*, $W_\infty = 0$, (a), and one situation of the *non-symmetrical case*, $W_\infty = -0.1$ (b).

In addition, the locations of maximum temperature values are shifted toward the region of the greater magnitudes of the lifting effect. Independently of the asymmetric factor value, an increase in the Joule heating parameter yields a more pronounced parabolic type curve. For example, an increment of ϕ^2 from 0.1 to 0.4 produces an increase in temperature of 100% at

the location $\xi=0$. In the case where the temperature values of the walls are interchanged, a mirror image of figures 5.2b will be obtained; however, this modification will have no effect in figure 5.2a.

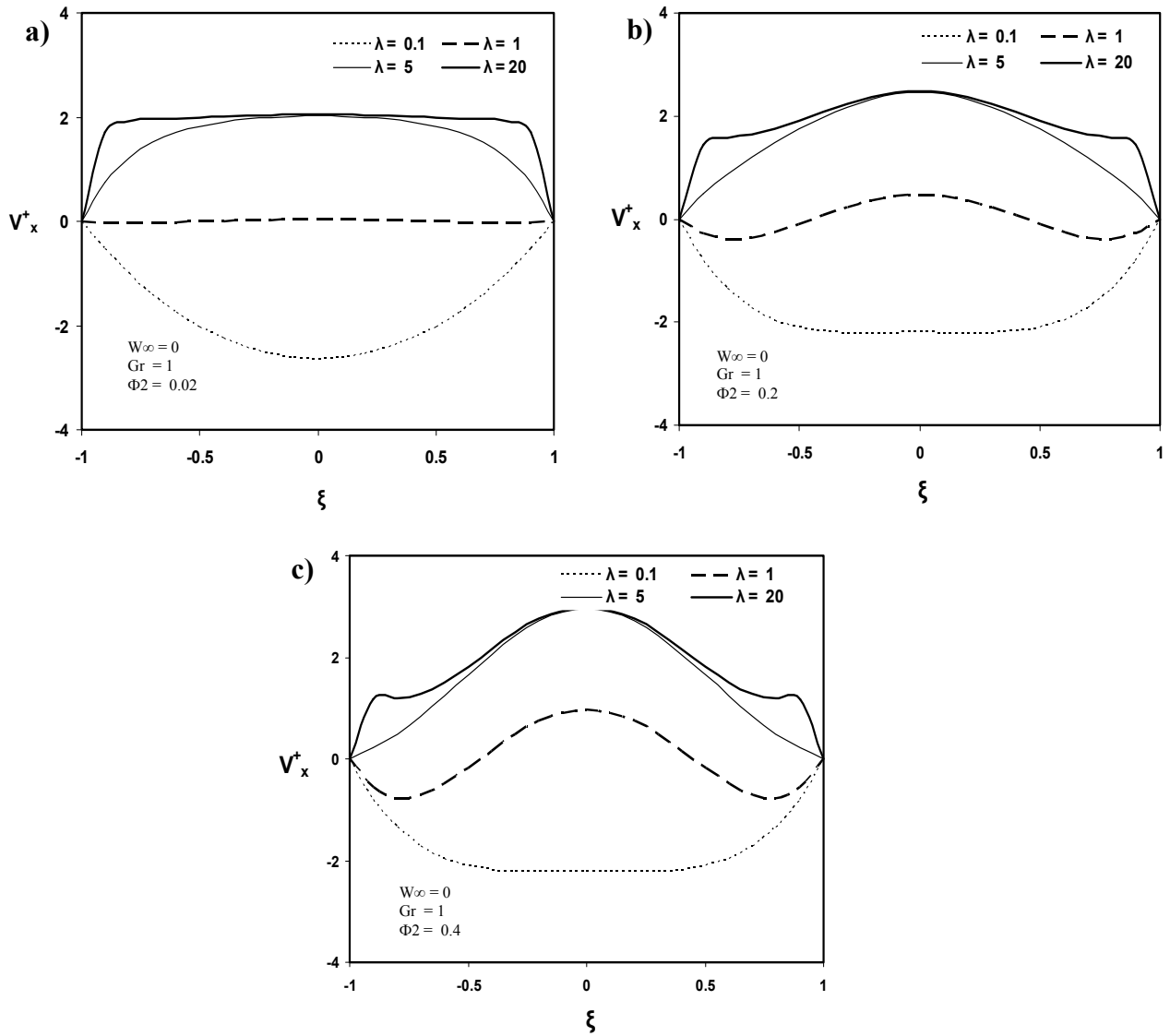


Figure 5.3 Typical hydrodynamic behavior of the physical system for the *symmetrical case* ($W_\infty=0$) for Grashof number $Gr=1$.

In order to illustrate the role of the asymmetric factor on the velocity profile two cases are studied. Asymmetric factor, $W_\infty = 0$, i.e. the symmetric case is examined in figure 5.3 for different values of the Joule heating number, $\phi^2 = 0.02$ (a); $\phi^2 = 0.2$ (b); and $\phi^2 = 0.4$ (c). In all the three situations, the dimensionless inverse Debye Hückel length, λ , is used as a parameter with the values indicated in the figure. The asymmetric factor $W_\infty \neq 0$ is analyzed in figure 5.4 (a,b&c) for the same values the Joule heating number used in the previous figure. Figures 5.3 (a,b&c) illustrate the effect of the Joule heating parameter on dimensionless velocity profiles along the transversal coordinate of the capillary. On this plot the Grashoff number has been held at the value of unity while the dimensionless Debye length is used as a parameter between $\lambda = 0.1$ and $\lambda = 20$. This particular range covers the most typical values of Debye lengths that have actual effect on the electrostatic potential and, therefore, on velocity. For low values of ϕ^2 (0.02) and λ (0.1) the system responded with a hydraulic-driven type curve. This implies that the Joule heating generation and electroosmosis effects are negligible. A flow reversal regime, dominated by electroosmosis, is reached when the parameter λ is increased from $\lambda = 0.1$ to $\lambda = 5$. An incipient partial flow reversal regime is present for the value of $\lambda = 1$ but it is not noticeable because of the scale used in the figure. An even more dominated electroosmotic flow regime is observed at high values of λ (20). As the Joule heating parameter is increased, illustrated in figures 5.3 b&c, the effects previously discussed are gradually magnified. For example, for $\phi^2 = 0.2$ the partial flow reversal regime is clearly observed in figure 5.3b and it is even more evident for the case of $\phi^2 = 0.4$ (Figure 5.3c). For the case of $\lambda = 5$ a deformation of the electroosmotic flow regime observed in figure 3a is clearly noticed in figure 5.3b due to induced buoyancy with higher values of the mean temperatures on the system. This particular trend is more pronounced in the case of $\phi^2 = 0.4$ (figure 5.3c). Now that the case of $W_\infty = 0$ has been examined, the attention is turned to the case of $W_\infty \neq 0$.

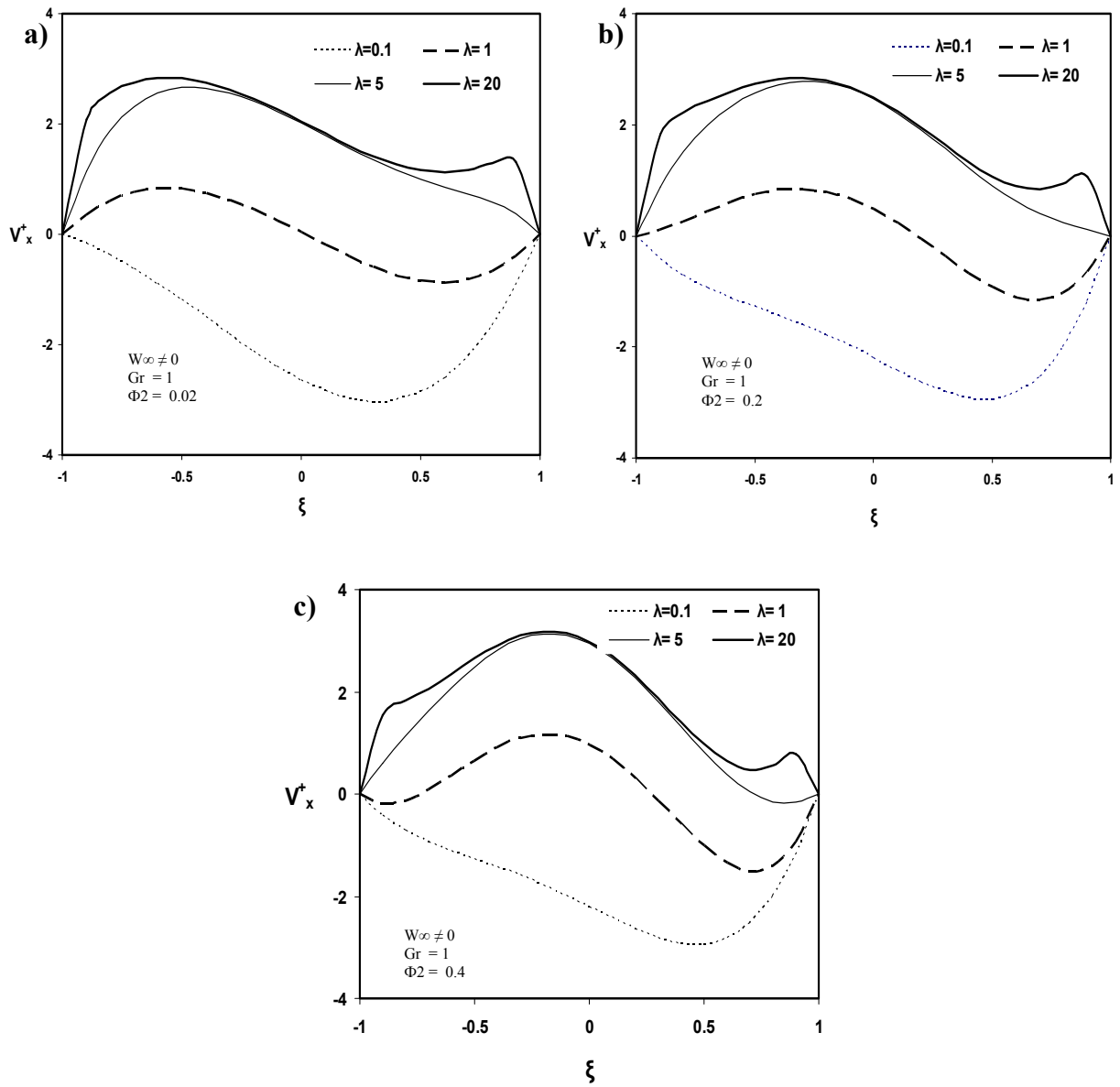


Figure 5.4 Typical hydrodynamic behavior of the physical system for one situation of the *non-symmetrical case* ($W_\infty = -0.1$) for Grashof number $Gr = 1$.

Figures 5.4 (a,b&c) describe the same variables as in figures 5.3 (a,b&c) however changing the asymmetric factor, W_∞ , to a value different from zero. As was observed in the temperature behavior when stressed by the effect of the asymmetric factor (see figure 5.2b), velocity profiles undergo strong deformation for all the cases of Joule heating generation and λ when the Grashoff number is held at the value of unity. More specifically, there is a clear loss of symmetry with respect to the flow regimes described previously for $W_\infty=0$. For example, for hydraulic-driven flow regimes, although the Joule heating effect is very low, maximum values of velocities, for all the cases, shift toward the wall with the lowest temperature value. On the other hand, for electroosmotic driven flow regimes ($\lambda =5$ and 20) the maximum values of velocities, for all the cases, shift toward the wall with the highest temperature value. Finally, for the case of flow regimes where the Joule heating effect is small ($\phi^2=0.02$) the buoyancy undergoes an amplified effect ($\lambda= 1$, see Figure 5.3a and 5.4a). For other flow regimes where buoyancy is present ($\phi^2=0.2$ and 0.4 , $\lambda= 1$) the values of maximum velocities shift to locations toward the wall with the highest temperature value as the minima move toward the opposite wall.

Another interesting analysis results from observing the hydrodynamic under low values of Grashoff number. The effect of buoyancy is attenuated or diminished for cases where the Grashoff number shows a lower value ($Gr = 0.01$, see figures 5.5 a,b&c). In fact, these figures show only a pressure-driven and an electroosmotic-driven family of flow regimes for all values of the Joule heating generation number. In which case, it is clearly observed that for fluids with low inverse Debye length the flow regime is pressure-driven. On the contrary, fluids with high inverse Debye length present an electroosmotic-driven behavior. Fluids with a moderated low inverse Debye length should be expected to present stagnation points.

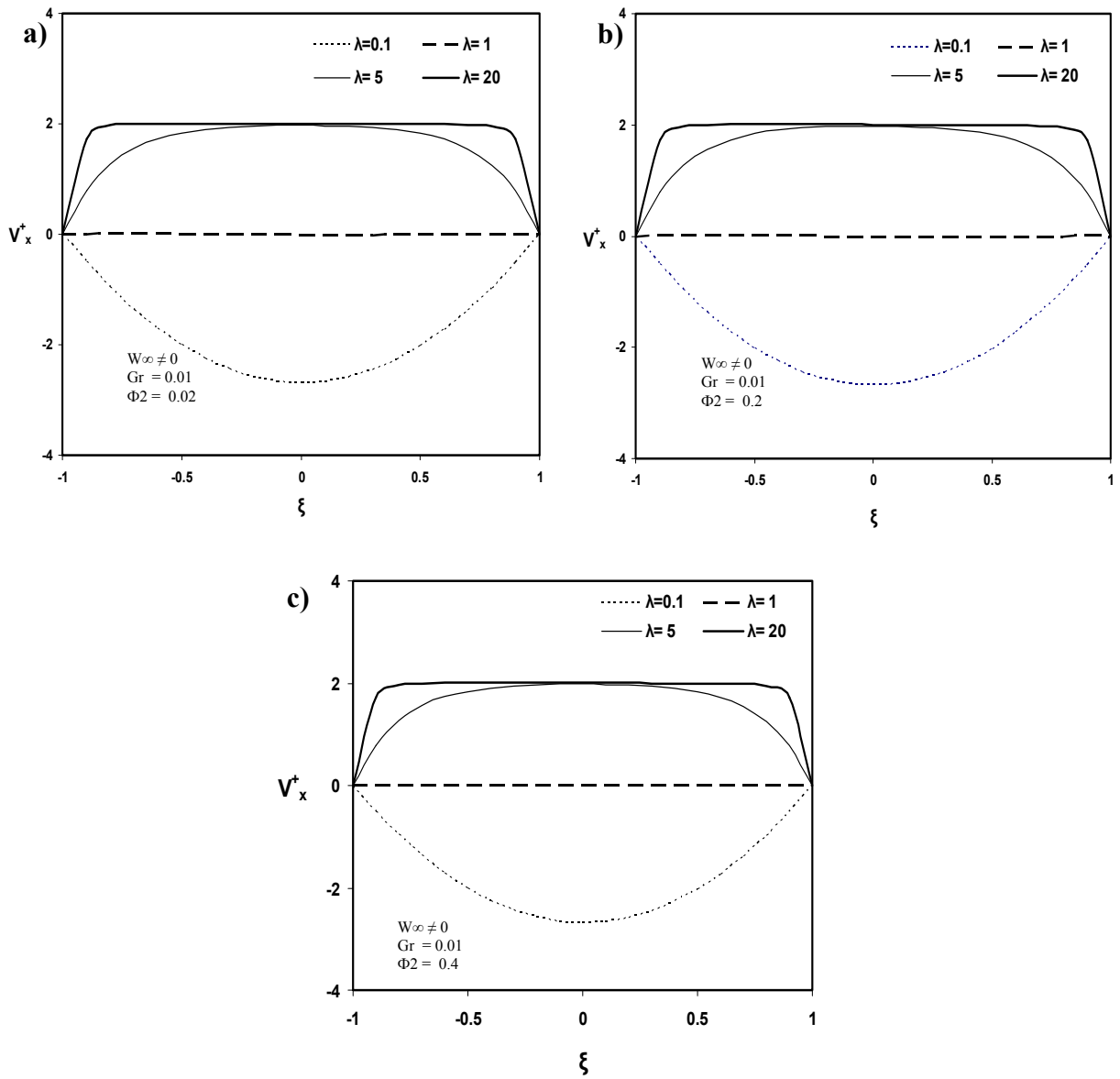


Figure 5.5 Typical hydrodynamic behavior of the physical system, for the *non-symmetrical case* ($W_\infty = -0.1$), for low influence of the buoyancy forces, Grashoff number $Gr = 10^{-2}$.

5.5 Summary of the Chapter

The present chapter was dedicated to studying the first target geometry and its related hydrodynamic aspects involved. Porous media have been simulated in a rectangular capillary to determine the different effect of the three main driving forces, found in electroremediation, on flow regime. To conduct the described task, this chapter was divided into sections that capture the main fundamental principles as well as the practical aspects and its results.

First, the interest of obtaining quantitative and semi-quantitative descriptions of the hydrodynamic yielded by a rectangular geometry is stated. With this, the main motivation and scope of the chapter are enunciated.

Second, the chapter describes the physical model and details of assumptions considered in a rectangular channel. Theoretical expressions are presented as well as their role in the mathematical description of the system under study. In particular, this chapter concentrates in developing the heat transfer and the conservation of momentum equations. The electrostatic model, also part of the system description, is only mentioned as the development was made in previous chapters.

Finally, the chapter illustrates with portrait results the different flow regime scenarios that could be obtained using the analytical solution of the fundamental equations describing the rectangular system. A comparison of driving forces is presented and the most characteristic cases are identified.